Composite Structures 242 (2020) 112097

Contents lists available at ScienceDirect

Composite Structures

journal homepage: www.elsevier.com/locate/compstruct

Mechanical behavior of thick composite tubes under four-point bending

Saeid Khadem Moshir, Suong V. Hoa*, Farjad Shadmehri, Daniel Rosca, Ashraf Ahmed

Concordia Center for Composites, Department of Mechanical, Industrial and Aerospace Engineering, Concordia University, Montreal, Quebec H3G 1M8, Canada

ARTICLE INFO

Keywords:
Stress analysis
Four-point bending
3D elasticity
Flexural stiffness
Strains
Finite element method
Experimental measurement

ABSTRACT

This paper presents the behavior of thick thermoplastic composite tubes made by an automated fiber placement machine, and subjected to four-point bending load. The mechanical behavior includes flexural stiffness, and strains. Methods for the determination of these behaviors include strength of material, analytical solution, finite element method and experimental measurement. The correlation between the different methods provides validation of some methods and indication of the degree of accuracy of some other methods. The accuracy of some calculating methods provides the ability to predict the performance of other thick composite tubes subjected to similar loading and support conditions.

1. Introduction

Having benefits over other materials in terms of light weight, high stiffness, high strength and good corrosion resistance, composite materials are being used more in many industries. One particular application of composites in the aerospace industry is the use of thermoplastic composite tubes as cross tubes for the landing gear in helicopters (ski type landing gears) (Fig. 1). This tube is subjected to four-point bending loading condition. These tubes have been made using aluminum. In order to reduce weight, thermoplastic composite tubes have been considered.

It was shown that it may be possible to design and make thermoplastic composite tubes that exhibit similar performance as that of an aluminum tube with 30% lighter weight [1–3]. These thermoplastic composite tubes have thick wall (about 12 mm thick) and containing many layers (100–200 layers). They are made by automated fiber placement and using carbon/PEKK thermoplastic composite materials. The results have been obtained using straight tubes and static loading conditions (3 points and 4 points bending). In order to make further advance in the technology, it is necessary to examine the analytical procedures that can be used to determine the mechanical performance of the tubes which include the flexural stiffness and strains. Toward this objective, the work described in this paper will first examine the different analytical techniques that have been developed for the determination of flexural stiffness, and strains in composite tubes subjected to four point bending loads. The results from the various analytical techniques are validated from experiments performed on a thick composite tube made by automated fiber placement machine.

2. Literature review

Many researches including theoretical as well as experimental methods to study mechanical behavior of composite cylinders and tubes subjected to axial tension, torsion, pressure, thermal load and pure bending have been carried out in the last three decades. Majority of them focused on stress analysis of thin tubes or tubes subjected to axisymmetric loads. Some of these works also studied tubes under hygrothermal and mechanical such as torque loads. Kollar and Springer [4] provided some formulations for a stress analysis of thin and thick-walled composite cylinders subjected to hygrothermal and mechanical loads (bending and torque). Their analysis is based on the equilibrium equations of Love [5] and applicable to loads which result in small deformation and linearly elastic material. The loads and therefore stresses and strains are independent of the axial coordinate. A displacement-based linear elasticity solution was used in order to study stress distribution and deformations in composite cylindrical tubes due to combined loading (internal and external pressure, torsion and axial load) by Tutunco and Winckler [6]. Hu et al. [7,8] employed Lekhnitskii's [9] stress functions to study stress distribution in a $\pm 55^{\circ}$ filament wound composite tube subjected to internal pressure or tension load.

A number of works have been done to study the mechanical behavior of composite tubes subjected to axisymmetric or thermomechanical loads. Pagano [10] presented a general solution for the elasticity problem of a homogeneous, hollow cylinder which is possessing cylindrical anisotropy under two-dimensional surface tractions in terms of a Fourier series in circumferential direction. A stress analysis of thick-walled concentric orthotropic cylinders subjected to internal pressure,

* Corresponding author.
E-mail address: hoasuon@alcor.concordia.ca (S.V. Hoa).

https://doi.org/10.1016/j.compstruct.2020.112097
Received 8 November 2019; Received in revised form 4 February 2020; Accepted 20 February 2020
Available online 25 February 2020
0263-8223/

Fig. 1. Cross piece for the ski type helicopter landing gear.

uniaxial tension or torsion based on the theory of Lekhnitskii [9] has been proposed by Davies and Bruce [11]. Han et al. [12] conducted a numerical study using LS-DYNA to evaluate the response and energy absorption capacity of composite tubes made of unidirectional pultruded tube over wrapped with ± 45 fiber reinforced plastic. The tubes subjected to both quasi-static compression and axial dynamic impact loadings. Akosy et al. [13] conducted stress analysis of laminated homogeneous cylinders subjected to thermal or inertia force due to rotation using 2D equilibrium equations in the cylindrical coordinate. However, they did not present any validation and also the effect of out-of-plane shear stresses as well as longitudinal stress were not considered. Nowak and Schmit [14] applied different methods such as theoretical, numerical and experimental analyses of fiber metal laminate tubes subjected to axisymmetric loads. A theoretical model at first was carried out to find a closed-form solution for a multi-layered cylinder subjected to thermomechanical load and then a finite element analysis was done to validate the results.

Some theoretical works have been carried out to study flexural behavior of the composite tubes subjected to pure bending loads. Stockwell and Cooper [15] investigated an extension of an approximate closed form solution of collapse of composite tubes subjected to end moments. They employed Reissners's simplified nonlinear analysis, in which it was assumed that the deformation of the tube cross-section is caused primarily by loading induced to the plane of the tube cross-section by the axial beam bending stress. When the tube bends, the axial stress follows the deformed shape, and a force is projected into the plane of the cross-section. Chan et al. [16] presented approaches based on laminate plate and shell theories to calculate the flexural stiffness of thin composite tubes. They also carried out finite element analysis using ANSYS to compare with theories. Tarn and Wang [17] applied an exact analytical solution to study extension, torsion, bending, anti-plane and in-plane shearing and pressuring of laminated composite tubes based on general expressions for the displacements of Lekhnitskii [9] and also the plane strain assumption was used. They formulated the basic equations of anisotropic elasticity in cylindrical coordinate system into a state equation by a judicious arrangement of the displacement and stress variables. Xia et al. [18] provided an exact solution based on classical laminate-plate theory for pure bending analysis of multi-layered filament-wound composite pipes based on Lekhnitskii's stress function. It is noted that the out-of-plane shear stress effects were not considered in their analysis. Arjomand and Taheri [19] employed finite element method (FEM) to study pure bending, nonlinear buckling and post-buckling of sandwich pipes. Menshykova and Guz [20] investigated stress analysis of multi-layered thick-walled fiber reinforced composite straight pipes manufactured by filament winding process under bending loading. They used the axial stress relation of Lekhnitskii then used stress–strain relation of Xia et al. [18]. Sun et al. [21] carried out a stress analysis of hollow cylindrical structures including multiple anisotropic layers using stress functions proposed by Lekhnitskii [9]. They also provided solutions for a homogenized composite cylinder with single-layer. Their solution is sufficient for stress analysis of thin-walled or moderately thick-walled hollow composite cylindrical structures. They compared the obtained results which were for composite tube with layers at winding angles other than 0 or 90° by the FEM. Jonnalagadda et al. [22] presented a simple analytical Euler-Bernoulli beam theory which works for thin-walled beam structures for a composite tube subjected to bending and torsion. The shear center distance of the tube (distance of the shear center from the tube axis) when it is subjected to torsional moment was obtained. They also carried out a finite element model using shell elements. Geuchy and Hoa [23] obtained flexural stiffness of two-layered thick composite tubes by utilizing three dimensional theory of elasticity proposed by Jolicoeur and Cardou [24]. They examined and compared theoretical results and experimental ones only for tubes with lay-up of [25/−25]. Akgun et al. [25] employed differential quadrature method to investigate nonlinear static behavior of laminated composite beams with hollow elliptical section subjected to three-point and end loading. The tubes have oval and elliptic cross sections which have adjusted parameters in the formulations (Lame curves). The nonlinearity is considered by applying von-Karman strain displacement relations. The first order shear deformation theory is used to take into account the shear effect. Also, the static equations were solved by employing the Newton-Raphson method. The out-of-plane shear stresses were not taken into account in their solution. Yazdani Sarvestani and Hojjati [26] employed a high-order displacement-based and the layer-wise method to investigate stresses and strains in thick laminated orthotropic tubes. Zhang and Hoa [29] extended the work of Jolicoeur and Cardou [26] to provide solution for tubes containing layers at all angles including 0 and 90°.

Most of the investigations studied mechanical behavior of composite tubes subjected to axisymmetric loadings such as extension loading, torsion, internal pressure or hygrothermal loadings. Various methods of analyses have been used for determining flexural stiffness and stress analysis of composite tubes under bending loading including FEM numerical method, 3D elasticity solution with Lekhnitskii's stress functions, thin-walled theory, shell theories and etc. Numerical methods such as FEM can be used but they are time consuming particularly for analyzing thick composite tubes with a large number of layers with different winding angles.

In summary, the vast majority of the previous works related to stress analysis of thick composite tubes under bending loading have been mainly analytical or numerical. There has been very limited experimental validation for these methods. A few experimental works have been done include the work of Saggar [19]. However, this Master thesis carried out four-point bending tests on tubes containing only 6 layers (about 0.9 mm thick) and therefore these are not particularly thick. These tubes have small diameters (from 0.375 in (9.5 mm) to 0.95 in 24.1 mm)) and as such they are small as compared to the cross tube for helicopter landing gears. Another publication on experimental work on composite tube was that of Blom et al. [20]. The focus of that work was to examine the effect of variable stiffness layers on the buckling performance of a composite cylinder, and not on the validation of theoretical method to determine stiffness and strains in thick composite tubes.

The main objective of the work presented in this paper is to provide experimental validation for the analytical methods such as strength of materials, the analytical method of Lekhnitskii and derivatives of this method, and finite element method, for the determination of flexural stiffness, and strains of thick composite tubes. With this validation, the less time consuming and less costly analytical methods may be used for the prediction of the behavior of other thick composite tubes subjected to similar loading and support conditions.

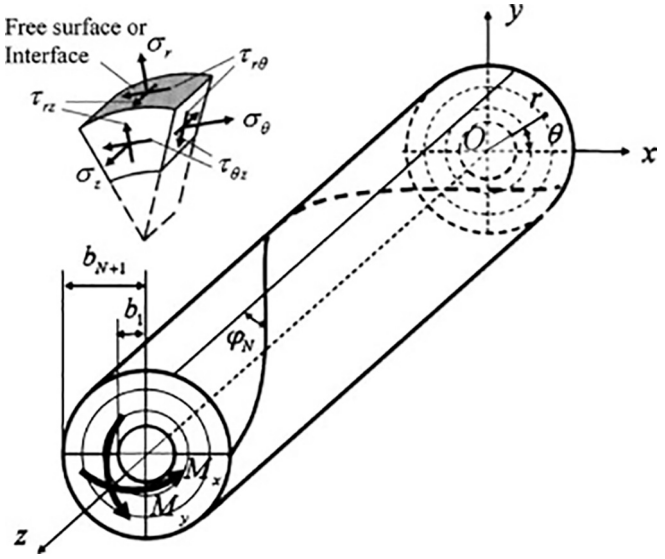

Fig.2. A composite tube subjected to pure bending [27].

3. The analytical and numerical methods

A composite tube consisting of different cylindrical layers (N) is shown in Fig. 2. The tube has elastic moduli E_1 and E_2 in fiber and transverse directions of each layer, respectively. The in-plane shear moduli and Poisson's ratios are G_{12}, G_{13}, ν_{12}, ν_{13} and the out-of-plane shear moduli and Poisson's ratio are G_{23} and ν_{23}, respectively. The tube with a winding angle of φ which is the angle between z axis and fiber direction is subjected to bending moments M_x and M_y. In the cylindrical coordinate system, r, θ and z are the radial, circumferential and longitudinal directions. The inside radius of each layer is denoted as b_n.

The analytical and numerical methods used for the determination of flexural stiffness, and strains have been strength of materials approach, Equations for thin walled composite tubes, 3D elasticity method by Lekhnitskii and derivatives, and finite element method. These are presented below.

3.1. Strength of materials equations [23]

The simplest method is the strength of materials approach. The flexural stiffness can be given as:

$$\langle EI \rangle = \sum_{n=1}^{N} \frac{\pi E_n}{4}(b_{n+1}^4 - b_n^4) \tag{1}$$

where E_n is the modulus along the axial direction for layer n. b_{n+1} and b_n are the outer radius and inner radius of layer n, respectively. E_n can be obtained from the elastic constants of the layer (E_1, E_2, G_{12}) and its fiber orientation θ as [28]:

$$E_x = \frac{E_1}{\cos^4\theta + \frac{E_1}{G_{12}}\sin^2\theta\cos^2\theta + \frac{E_1}{E_2}\sin^4\theta} \tag{2}$$

3.2. Thin-walled composite tubes [29]

In the thin-walled composite beam theory provided by Librescu and Song [30], in a unified way, a number of necessary effects in the design of composite thin-walled structures such as transverse shear deformation, torsion related nonuniform warping and secondary warping which are assumed to vary across the thickness are taken into consideration [31]. Based on the formulations provided by Shadmehri et al. [29], the flexural stiffness of composite tubes can be determined as follows

$$\langle EI \rangle = \frac{a_{33}a_{44} - a_{34}^2}{a_{44}} \tag{3}$$

where

$$\begin{aligned} a_{33} &= \pi R(K_{11}R^2 + 2RK_{14} + K_{44}) \\ a_{44} &= \pi R(A_{44} + K_{22}) \\ a_{34} &= -\pi R(K_{12}R + K_{24}) \end{aligned} \tag{4}$$

R is the average radius of the tube, and we have

$$\begin{aligned} K_{11} &= A_{22} - \frac{A_{12}(A_{33}A_{12} - A_{13}A_{23})}{\overline{A}} - \frac{A_{23}(A_{23}A_{11} - A_{13}A_{12})}{\overline{A}} \\ K_{14} &= B_{22} - \frac{A_{12}(A_{33}B_{12} - A_{13}B_{23})}{\overline{A}} - \frac{A_{23}(A_{11}B_{23} - A_{13}B_{12})}{\overline{A}} \\ K_{44} &= D_{22} - \frac{B_{12}(A_{33}B_{12} - A_{13}B_{23})}{\overline{A}} - \frac{B_{23}(A_{11}B_{23} - A_{13}B_{12})}{\overline{A}} \\ K_{22} &= A_{66} - \frac{A_{16}(A_{33}A_{16} - A_{13}A_{36})}{\overline{A}} - \frac{A_{36}(A_{11}A_{36} - A_{13}A_{16})}{\overline{A}} \\ K_{12} &= A_{26} - \frac{A_{12}(A_{33}A_{16} - A_{13}A_{36})}{\overline{A}} - \frac{A_{23}(A_{36}A_{11} - A_{13}A_{16})}{\overline{A}} \\ K_{24} &= B_{24} - \frac{A_{16}(A_{33}B_{12} - A_{13}A_{23})}{\overline{A}} - \frac{A_{36}(A_{11}B_{23} - A_{13}B_{12})}{\overline{A}} \end{aligned} \tag{5}$$

In which, $A_{ij} = \int_{-h/2}^{h/2} \overline{C}_{ij}dz$, $B_{ij} = \int_{-h/2}^{h/2} \overline{C}_{ij}zdz$, $D_{ij} = \int_{-h/2}^{h/2} \overline{C}_{ij}z^2dz$ are laminate stiffness constants, h is the thickness of each layer, and $\overline{A} = A_{11}A_{33} - A_{13}^2$.

In this approach, it is assumed that all deformations are small and the in-plane deformations are not allowed in the cross-section plane.

3.3. Analytical 3D elasticity method of Lekhnitskii [9], Jolicoeur and Cardou [24], Zhang and Hoa [27]

The fundamental equations of an analytical mathematical approach were provided by Lekhnitskii [9] for the first time. He derived a set of partial differential equations for an isotropic cylinder under axisymmetric loading. Following this approach, a coaxial hollow circular orthotropic cylinder subjected to combined bending, tensile and torsion loads was analyzed analytically by Jolicoeur and Cardou [24] in order to obtain stresses, flexural stiffness as well as displacements. Two types of no-slip and no-friction condition between layers were considered. According to constitutive equations in this approach, the flexural stiffness for a composite tube can be calculated by the following formula

$$(EI) = \sum_{n=1}^{N} \frac{\pi}{C_{33,n}} \left\{ \begin{array}{c} K_{i,n}[C_{34,n}g_{i,n}m_{i,n} - C_{13,n} - C_{23,n}(m_{i,n}+1)] \\ \sum_{i=1}^{4} \left[\frac{b_{n+1}^{m_{i,n}+2} - b_n^{m_{i,2}+2}}{m_{i,n}+2} \right] \\ + \left[1 - \mu_{1,n}(C_{13,n} + 3C_{23,n}) + 2\mu_{2,n}C_{34}\left(\frac{b_{n+1}^4 - b_n^4}{4}\right) \right] \end{array} \right\} \tag{6}$$

where, b_n and b_{n+1} are the internal and external radii of a cylinder, n is the index of each cylinder. K_i are four arbitrary constants and

$$g_i = \frac{\beta_{24}m_i^2 + (\beta_{14} + \beta_{24})m_i - \beta_{56}}{\beta_{44}m_i^2 - \beta_{55}} \tag{7}$$

C_{ij} (i,j = 1..6) are material property constants [32] and β_{ij} are reduced elastic constants defined by Lekhnitskii [24] in terms of elastic constants C_{ij} can be expressed as follow

$$\beta_{ij} = C_{ij} - \frac{C_{i3}C_{3j}}{C_{33}} \tag{8}$$

m_i are roots of the characteristic equation as in the following form [24]

$$m_{1..4} = \pm\sqrt{\frac{-b \pm \sqrt{b^2 - 4ac}}{2a}} \tag{9}$$

where

$$a = \beta_{22}\beta_{44} - \beta_{24}^2$$
$$b = \beta_{24}(2\beta_{14} + \beta_{24} + 2\beta_{56}) - \beta_{44}(\beta_{11} + 2\beta_{12} + \beta_{22} + \beta_{66}) - \beta_{22}\beta_{55} + \beta_{14}^2$$
$$c = \beta_{55}(\beta_{11} + 2\beta_{12} + \beta_{22} + \beta_{66}) - \beta_{56}^2 \tag{10}$$

and

$$\begin{Bmatrix}\mu_1\\ \mu_2\end{Bmatrix} = \begin{bmatrix} -2\beta_{14} - 6\beta_{24} + \beta_{56} & 2\beta_{44} - \beta_{55} \\ -\beta_{11} - 2\beta_{12} + 3\beta_{22} - \beta_{66} & 2\beta_{14} - 2\beta_{24} + \beta_{56}\end{bmatrix}^{-1} \frac{1}{C_{33}} \begin{Bmatrix} 2C_{34} \\ C_{13} - C_{23}\end{Bmatrix} \tag{11}$$

By utilizing continuity conditions at interfaces for either no-slip or no-friction cases, the bending stiffness of the composite tube can be obtained. Also, the in-plane and out-of-plane stresses for either no-slip or no-friction cases can be expressed as

$$\sigma_r = (\kappa_x \sin(\theta) - \kappa_y \cos(\theta))\left(\sum_{i=1}^{4} K_i r^{m_i - 1} + \mu_1 r\right) \tag{12}$$

$$\sigma_\theta = (\kappa_x \sin(\theta) - \kappa_y \cos(\theta))\left(\sum_{i=1}^{4} K_i (m_i + 1) r^{m_i - 1} + 3\mu_1 r\right) \tag{13}$$

$$\sigma_z = \frac{1}{C_{33}}(\kappa_x r \sin(\theta) - \kappa_y r \cos(\theta) - C_{13}\sigma_r - C_{23}\sigma_\theta - C_{34}\tau_{\theta z}) \tag{14}$$

$$\tau_{r\theta} = (\kappa_x \cos(\theta) + \kappa_y \sin(\theta))\left(-\sum_{i=1}^{4} K_i r^{m_i - 1} - \mu_1 r\right) \tag{15}$$

$$\tau_{rz} = (\kappa_x \cos(\theta) + \kappa_y \sin(\theta))\left(\sum_{i=1}^{4} K_i g_i r^{m_i - 1} + \mu_2 r\right) \tag{16}$$

$$\tau_{\theta z} = (\kappa_x \sin(\theta) - \kappa_y \cos(\theta))\left(-\sum_{i=1}^{4} K_i g_i m_i r^{m_i - 1} - 2\mu_2 r\right) \tag{17}$$

In which k_x and k_y are the bending curvatures of the center line.

It was realized by Zhang et al. [27] that in the method provided by Jolicoeur and Cardou [24] some of parameters are singular when the tube includes 0° and 90° layer orientations although the stresses and displacement are nonsingular. Therefore, the continuity condition between 0° layers or 90° layers and other ordinary layers cannot be performed. In order to overcome this issue, Taylor series expansions were applied to obtain parameters for winding angles of the tube including (0° or 90°), [27]. In this method, the flexural stiffness may be calculated as follows

$$\begin{aligned}(EI) = \sum_{n=1}^{N} \frac{\pi}{C_{33,n}} \Bigg\{ & \sum_{i=1}^{2} K_{i,n}(C_{13,n} + C_{23,n}(m_{i,n} + 1) \\ & - C_{34,n} m_{i,n} g_{i,n}) \frac{b_n^{m_{i,n}+2} - b_{n+1}^{m_{i,n}+2}}{m_{i,n} + 2} \\ + \sum_{j=3}^{4} K_{j,n}^* (C_{13,n} g_{j,n}^* & + C_{23,n}(m_{j,n} + 1) g_{j,n}^* - C_{34,n} m_{j,n}) \frac{b_n^{m_{j,n}+2} - b_{n+1}^{m_{j,n}+2}}{m_{j,n} + 2} \\ & + (\mu_{1,n}(C_{13,n} + 3C_{23,n}) - 2\mu_{2,n} C_{34,n} - 1) \frac{b_n^4 - b_{n+1}^4}{4}\end{aligned} \tag{18}$$

where $i = 1, 2$ and $j = 3, 4$. The unified coefficients can be introduced as

$$K_j^* = \begin{cases} K_j g_j & \varphi \neq 90 \ or \ 0 \\ \widetilde{K_j g_j} & \varphi = 90 \ or \ 0 \end{cases} \quad j = 3, \ 4 \tag{19}$$

The symbol $\sim$ represents the limit. The corresponding parameters can be introduced as

$$g_i^* = \begin{cases} g_j^{-1} & \varphi \neq 0 \text{ or } 90 \\ 0 & \varphi = 0 \text{ or } 90 \end{cases} \quad \text{j= 3, 4} \tag{20}$$

It should be noted that for the 0° or 90° layers, $g_3^* = g_4^* = 0$ by using Eq. (19) then the K_3^* and K_4^* for special layers can be derived by using the continuity condition rather than by using Eq. (20).

The g_3 and g_4 at special layers 0° or 90° cannot be calculated straightforwardly because the denominator of g_i are equal to zero. So that for special layers such as (0° or 90°) the variables g_3 and g_4 (j = 3, 4) cannot be derived easily using their Taylor series expansion. In other meaning, for special layers such as 0 or 90° layers, the g_3 and g_4 will be infinite, in order to eliminate this singularity, their limit should be used. Also, $\widetilde{K_3 g_3}$ and $\widetilde{K_4 g_4}$ have to be considered together instead of single K_3, K_4 and g_3, g_4 because $\widetilde{g_3}$ and $\widetilde{g_4}$ are infinite in $|\lim_{\varphi \to 0,90} g_3| = \infty$ and $|\lim_{\varphi \to 0,90} g_4| = \infty$.

It is noted that in the case of no-slip condition between the layers (i.e. there is perfect bonding between layers), there is continuity of stresses σ_r, $\tau_{r\theta}$ and τ_{rz} and of displacements u_r, u_θ and w. On the other hand, in the case of no-friction condition, there is some discontinuity of u_θ and w. It means that longitudinal as well as tangential slip between layers are allowed.

By applying boundary conditions at inner and outer surfaces of the tube and continuity condition at the interface between the layers, the constants $K_{1,n}$, $K_{2,n}$, $K_{3,n}^*$ and $K_{4,n}^*$ can be determined. The in-plane as well as out-of-plane stresses can be as the following

$$\sigma_r = (\kappa_x \sin(\theta) - \kappa_y \cos(\theta))\left(\sum_{i=1}^{2} K_i r^{m_i - 1} + \sum_{j=3}^{4} K_j^* g_j^* r^{m_j - 1} + \mu_1 r\right) \tag{21}$$

$$\sigma_\theta = (\kappa_x \sin(\theta) - \kappa_y \cos(\theta))\left(\sum_{i=1}^{2} K_i (m_i + 1) r^{m_i - 1} + \sum_{j=3}^{4} K_j^* g_j^* (m_j + 1) r^{m_j - 1} + 3\mu_1 r\right) \tag{22}$$

$$\sigma_z = \frac{1}{C_{33}}(\kappa_x r \sin(\theta) - \kappa_y r \cos(\theta) - C_{13}\sigma_r - C_{23}\sigma_\theta - C_{34}\tau_{\theta z}) \tag{23}$$

$$\tau_{r\theta} = (\kappa_x \cos(\theta) + \kappa_y \sin(\theta))\left(-\sum_{i=1}^{2} K_i r^{m_i - 1} + \sum_{j=3}^{4} K_j^* g_j^* r^{m_i - 1} - \mu_1 r\right) \tag{24}$$

$$\tau_{rz} = (\kappa_x \cos(\theta) + \kappa_y \sin(\theta))\left(\sum_{i=1}^{2} K_i g_i r^{m_i - 1} + \sum_{j=3}^{4} K_j^* r^{m_j - 1} + \mu_2 r\right) \tag{25}$$

$$\tau_{\theta z} = (\kappa_x \sin(\theta) - \kappa_y \cos(\theta))\left(-\sum_{i=1}^{2} K_i g_i m_i r^{m_i - 1} - \sum_{j=3}^{4} K_j^* m_j r^{m_j - 1} - 2\overline{\mu}_2 r\right) \tag{26}$$

In these methods, all the stresses are taken into consideration and the distribution of stresses in the thickness of the tube can be achieved.

4. Finite element analysis

In order to investigate the stress analysis of composite tube, the FEM (ANSYS) can be used. The element Solid 185 with 8 nodes and three degrees of freedom at each node can be implemented for the analysis. The total number of elements in the longitudinal, circumferential as well as thickness directions are 105 × 67 × 43, respectively.

In the modeling, the tube is under four-point bending loading. For the loading simulation, nodes in half of the circle (180°) on the surface of the tube are subject to vertical loading. For the simulation of the support conditions (also covering 180° of the circumference of the tube), the displacements in the x, y and z directions are zero at one end, and at the other end, the displacements in the x and y directions are zero and in the z direction, the nodes are free.

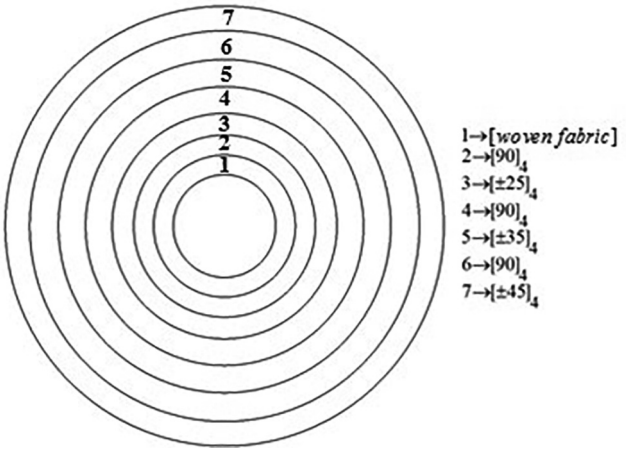

Fig. 3. Composition of the thickness of the tube.

5. Experiments

5.1. Fabrication of the composite tube

In order to obtain experimental values to validate the results obtained from the analytical and numerical methods, a straight composite tube was made and tested. The tube was made using an automated fiber placement (AFP) machine available at Concordia Center for Composites. In order to process thermoplastic composites, a hot gas torch was used to melt the thermoplastic resin so that consolidation can be done in-situ. The mandrel needs to be sufficiently stiff to support the compaction load exerted by the placement head of the machine. Another requirement is that the mandrel should be removable to assure the lightness of the final structure. In order to satisfy these requirements, a layer of woven fabric was used on the inner side of the tube. As such the thickness of the tube has the composition as shown in Fig. 3.

The composite tube lay-up has 7 layers of Carbon/Epoxy five-harness satin woven fabric with the thickness of each layer 0.285 mm, and 36 layers made of Carbon/PEEK thermoplastic (average layer thickness of 0.115 mm), with the following lay sequence:

$$[(5Harness\ satin)_7/90_4/(\pm25)_4/90_4/(\pm35)_4/90_4/(\pm45)_4]$$

The total thickness of the tube is 6.14 mm.

This lay up sequence follows the strain controlled design guidelines developed in [1] where the outer layers should possess larger strain to failure as compared to the inner layers, and the $[90_n]$ layers are used to buffer the effect of transmission of failure from layers with smaller deformation capability to layers of larger deformation capability.

The tube has the length $L = 1352.4$ mm, inner and outer diameters $Di = 72.71$ mm and $Do = 85$ mm, respectively. The material properties of woven fabrics and unidirectional Carbon/PEEK are shown in Tables 1 and 2, respectively.

Table 1
Mechanical properties of 5-harness satin, [33].

E_1 (GPa)	54
E_2 (GPa)	54
E_3 (GPa)	9.964
G_{12} (GPa)	4
G_{13} (GPa)	2.50
G_{23} (GPa)	2.5
ν_{12}	0.05
ν_{13}	0.254
ν_{23}	0.289

Table 2
Mechanical properties of unidirectional Carbon/PEEK composite, [34].

E_1 (GPa)	138
$E_2 = E_3$ (GPa)	10.2
$G_{12} = G_{13} = G_{23}$ (GPa)	5.7
$\nu_{12} = \nu_{13}$	0.31
ν_{23}	0.33

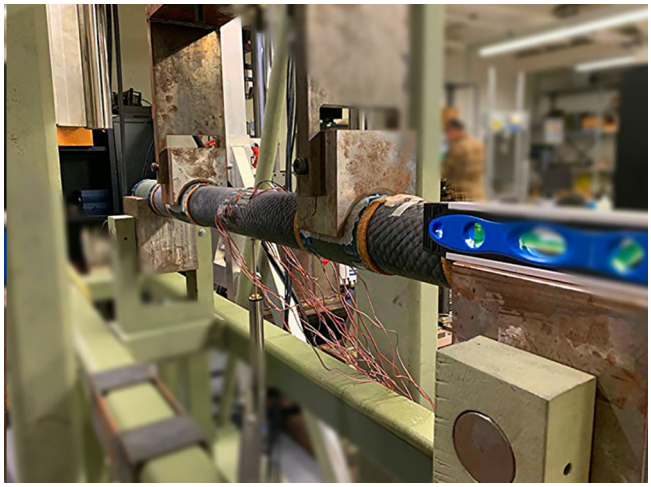

Fig. 4. Composite tube in a tube bending test set up.

5.2. Four-point bending test

The tube is subjected to four-point bending loading arrangement as shown in the Fig. 4. The loading noses and the supports have concave shape which cover 180° of the circumference. The supports and the loading noses are made of steel. The supports can rotate around x axis.

Six rosette strain gauges are installed at the mid-length, on the outer surface of the tube and at circumference positions $\theta = 0^\circ, 45^\circ, 90^\circ, 135^\circ, 180^\circ, 270^\circ$(coordinate axes shown in Fig. 5). Table 3 shows the positions of the gauges which are located at the outer surface of the tube, at section A-A. Two T type strain gauges are installed at sections B-B and C–C of the tube.

6. Results

6.1. Flexural stiffness

Value of the flexural stiffness can be determined using the equivalent product $< EI >$, where E stands for modulus of elasticity and I for cross section inertia.

- Strength of materials approach: Using Eq. (1): $\langle EI \rangle = 33 \times 10^3$ N. m^2
- Thin walled composite tubes: Using Eq. (3): $\langle EI \rangle = 62 \times 10^3$ N. m^2
- 3D elasticity (Lekhnitskii): Using Eq. (6): (no-slip condition) $\langle EI \rangle = 57.5 \times 10^3$ N. m^2
- 3D elasticity (Lekhnitskii): Using Eq, (6): (no-friction condition): $\langle EI \rangle = 32.7 \times 10^3$ N. m^2
- Experiment: $<EI> = \frac{MR}{\varepsilon} = \frac{MD_o}{2\varepsilon} = \frac{F(a+e-c-d)D_o}{8\varepsilon}$ where

Do is the outer diameter of the tube
a is the length between support points
d is width of the load pad
e is width of the support pad
c is the length between loading points
F is the machine load
ε is the axial strain at mid length of the tube, either at the bottom or

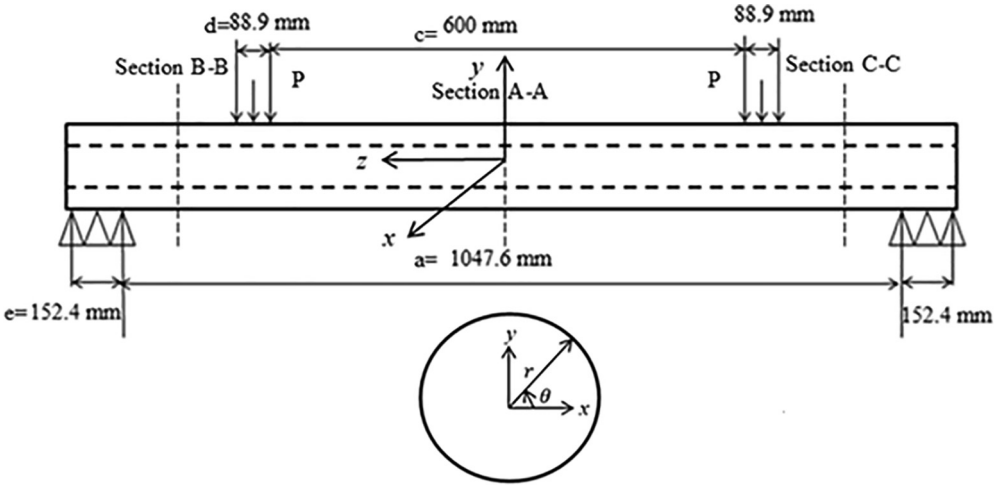

Fig. 5. Schematic of composite tube under four-points bending loadings.

Table 3
Locations of strain gauges on the surface of the tube, Section A-A.

Rosette No.	Channel No.	Z (mm)	θ (degree)	Strain gauge angle with z
1	1	0	88	90
	2	0	90	45
	3	0	92	0
2	4	−1	132	90
	5	−1	134	45
	6	−1	136	0
3	7	−0.5	179	90
	8	−0.5	180	45
	9	−0.5	182	0
4	10	0	272	90
	11	0	270	45
	12	0	268	0
5	13	−1	359	90
	14	−1	360	45
	15	−1	2	0
6	16	−0.5	44	90
	17	−0.5	46	45
	18	−0.5	48	0

top

F/ε is obtained from the slope of the load versus axial strain either at the bottom or top of the tube.

From the above: $\langle EI \rangle = 58.1 \times 10^3$ N.m^2

6.2. Strains

Fig. 6 shows the experimental strains at θ = 0° (rosette # 5) and θ = 180° (rosette # 3). The calculated values show that these strains are 0. Reasons for this are presented in the Discussion section below.

Fig. 7 shows the strain variations at θ = 45°. (strain rosette # 6), and Fig. 8 shows the strains at θ = 135° (rosette # 2). These two positions are nominally symmetrical with respect to the vertical axis of the cross section. It can be observed from these two figures that the calculated values are the same. However the longitudinal strains in Fig. 7 are larger than the calculated strains while those in Fig. 8 are smaller than the calculated strains. Reasons for this are given in the Discussion section below.

Fig. 9 shows the variation of the strains at θ = 90° (strain rosette # 1, top of the section), and Fig. 10 shows the strains at θ = 270° (rosette # 4, bottom of the section). Results obtained from 3D elasticity solution (no-slip condition), FEM, and experiments are shown. It can be seen that the results agree very well.

Fig. 11 shows the strains variation at θ = 90°, section B-B, (T#1)

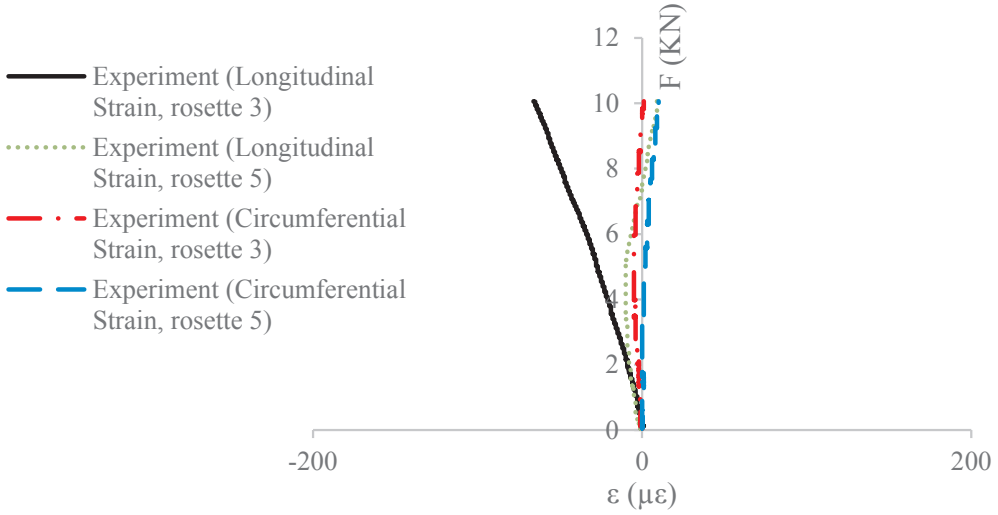

Fig. 6. Longitudinal and circumferential strains versus load F at $\boldsymbol{\theta} = 0°$ and $\boldsymbol{\theta} = 180°$ (F = 2P). (Strains from rosettes 3 and 5).

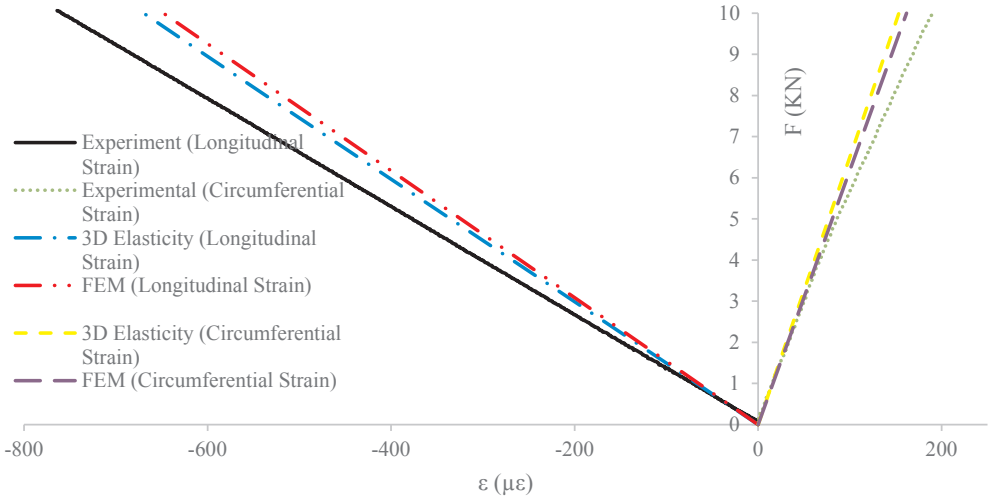

Fig. 7. Longitudinal and circumferential strains versus machine loading at $\boldsymbol{\theta}$ = 45°, (rosette # 6) (F = 2P).

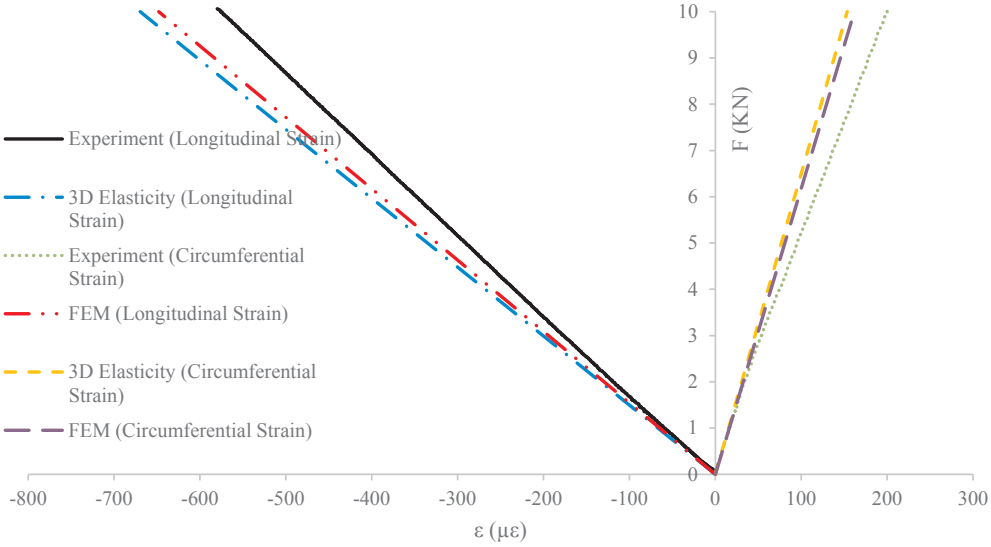

Fig. 8. Longitudinal and circumferential strains versus load F at $\boldsymbol{\theta}$ = 135°, (F = 2P), **(rosette # 2)**.

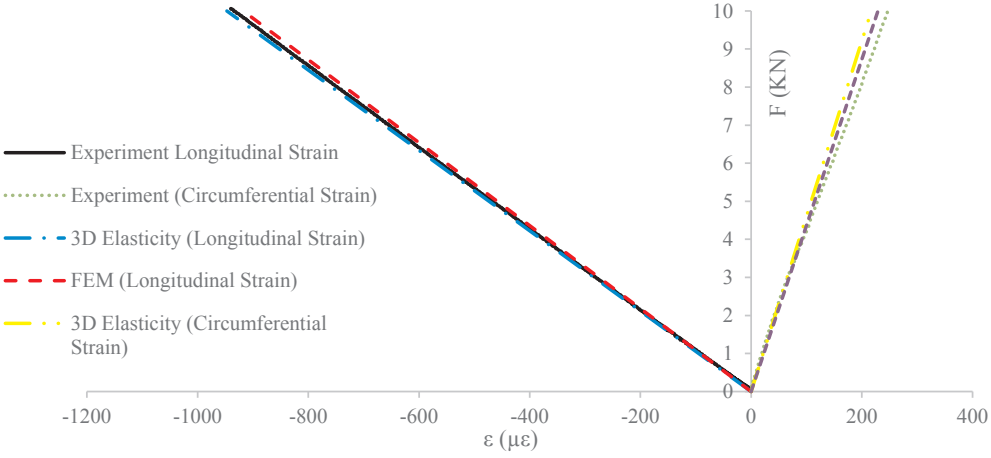

Fig. 9. Longitudinal and circumferential strains versus load F at $\boldsymbol{\theta}$ = 90°, (F = 2P).

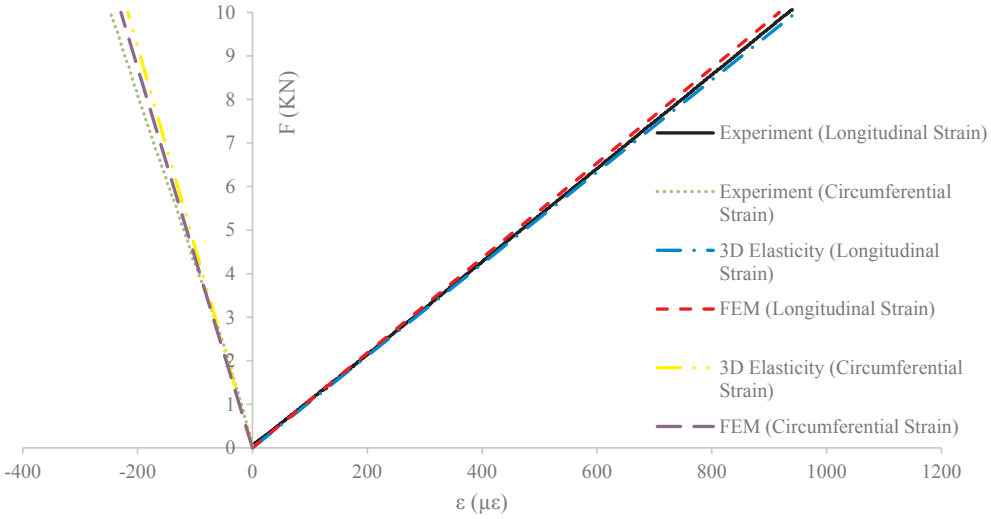

Fig. 10. Longitudinal and circumferential strains versus machine loading at $\boldsymbol{\theta}$ = 270°, (rosette # 4) (F = 2P).

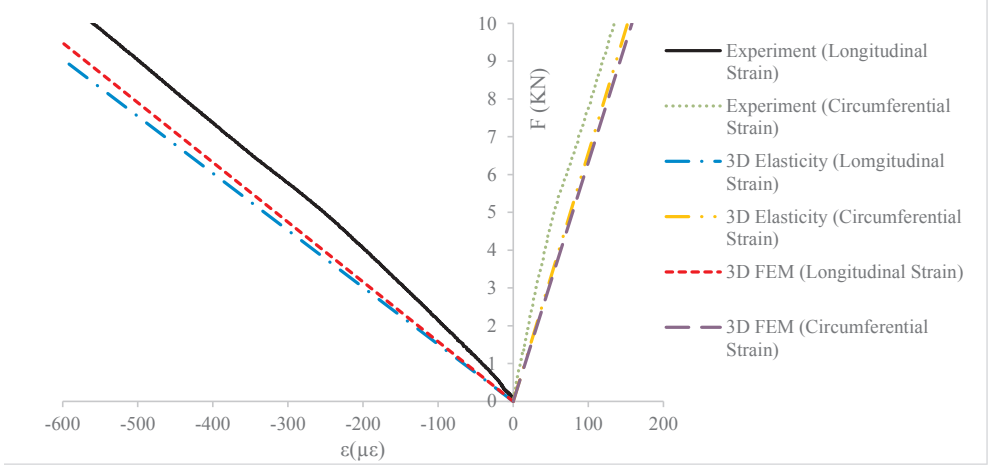

Fig. 11. Longitudinal and circumferential strains versus machine loading at $\boldsymbol{\theta}$ = 90°, (Section B-B, rosette # T1), (F = 2P).

Table 4
Locations of strain gauges on the surface of the tube, Sections B-B, and C–C.

T type No.	Channel No./Type	z (mm)	r (mm)	θ (degree)
T1	20/hoop	431.8	42.5	90
	21/axial	431.8	42.5	90
T2	22/hoop	−431.8	42.5	90
	23/axial	−431.8	42.5	90

7. Discussion

7.1. Flexural stiffness:

- There is general agreement between values obtained using thin walled theory (Eq. (3)), 3D elasticity (Eq. (6) using no-slip condition), and experimental measurement. Values of < EI > obtained from these methods vary from 57,500 N.m^2 to 62,000 N.m^2, giving an average of 59,200 N.m^2 with deviation of 4.7%.
- The strength of materials solution (Eq. (1)) seems to agree with the 3D elasticity solution (Eq. (6) using no friction condition). The EI values are 33,000 N.m^2 and 32,700 N.m^2 which are very close. However these values are much smaller than the experimental value. No friction condition means that the layers are not bonded together, which is far from reality.

7.2. Strains

- Fig. 6 shows the strains at θ = 0° and 180°, which are the horizontal positions of the section. It is expected that the strains be close to 0. Rosette # 3 show small values because it is located at θ = 182° which is slightly away from 180°.
- Figs. 7 and 8 show the strains at θ = 45° (rosette # 6) and 135° (rosette # 2). These are supposed to be symmetric positions on the tube. However, the longitudinal strains at θ = 45° are larger than the calculated strains while those at θ = 135° are smaller than the calculated strains. Examination of Table 3 shows that the axial gage in rosette # 6 is located at θ = 48° while that of rosette # 2 is located at θ = 136°. The distance from the neutral axis of the axial strain in rosette # 6 is more than that of the axial strain in rosette # 2. This may explain the larger amplitude in the gage at the nominal θ = 45°.
- Figs. 9 and 10 show the strains at θ = 90° (rosette # 1, top of section) and at θ = 270° (rosette # 4, bottom of the section). There is good agreement between the 3D elasticity solution, FEM solution and experimental measurement.
- The above analysis shows that the analytical methods (3D analytical with no-slip condition, and FEM) can predict the strains well. The small differences can be explained due to the slight deviation of the position of the gages as compared to the theoretical positions. Between 3D analytical and FEM, 3D analytical is simpler and less

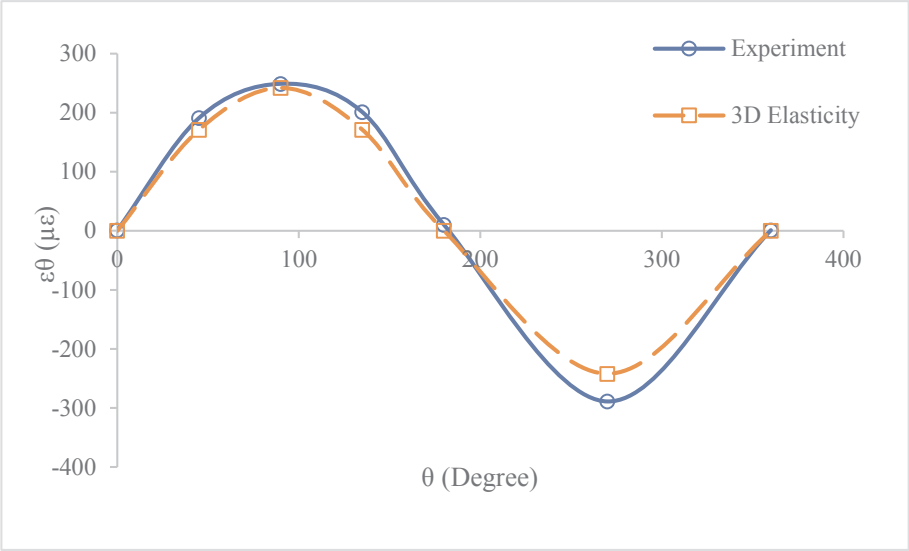

Fig. 12. Variation of the circumferential strain versus circumference at the outer surface of the tube, mid-length. (F = 10 KN).

time consuming.

- It is of interest to compare the experimental longitudinal strains from Figs. 9 and 11. Fig. 9 shows the strain from rosette # 1 which is at the top and mid length of the tube. This is the region of pure bending. Fig. 11 shows the strain from T1 gage at section B-B, which is at the top of the cylinder but located within the region where there is a bending moment and a shear load. From Table 4 and Fig. 5, it can be shown that the bending moment at section B-B is $M_{B\text{-}B}$ = (168.2 mm) P, and the pure bending moment at section A-A is $M_{A\text{-}A}$ = (255.6 mm)P. At a load F = 10 kN, Fig. 9 shows a longitudinal experimental strain of about −940 με while Fig. 11 shows a longitudinal experimental strain of about −565 με. The ratio between the bending moments is (255.6/168.2 = 1.52) while the ratio between the two strains is (940/565 = 1.66). If one were to use the section A-A under pure bending moment as the reference, the strain due to bending at section B-B would be (−940)(168.2)/(255.6) = -618.6 με. The difference between −618.6 με and −565με (53.6 με) is due to the presence of the shear load at section B-B. The ratio (53.6/618.6 = 8.7%) represents the relative importance of shear with respect to bending moment.
- It is of interest to see the variation of the circumferential strain along the circumferential direction. This can be done by plotting the calculated circumferential strains at different θ values. Fig. 12 shows the variation. It can be seen that at the top of the section A-A, the longitudinal strain is compressive while the circumferential strain is tensile. The opposite occurs at the bottom of the section.

8. Conclusion

In this paper, the different methods developed for the determination of flexural stiffness and strains in thick composite tubes subjected to four-point bending have been evaluated using experimental results obtained from testing a thick composite tube. The thick composite tube was made using carbon/PEEK thermoplastic composite material, and an automated fiber placement machine. The tube has a thickness of more than 5 mm.

It was shown that for flexural stiffness, the thin walled theory, 3D elasticity (with no slip condition), FEM method show results that agree well with experimental values, while the strength of materials approach, and 3D elasticity (with no friction condition) agree with each other but both give flexural stiffness values much lower than the experimental values.

For strains, it is also shown that the analytical method (3D elasticity solution with no slip condition), and FEM can obtain results that agree with experimental measurement. Among the calculated method, 3D elasticity solution is less time consuming, and more simple.

The strains at sections where there is a combination of bending moment and a shear load shows that there is significant influence of the shear load on the strains.

CRediT authorship contribution statement

Saeid Khadem Moshir: Formal analysis, Methodology. **Suong V. Hoa:** Conceptualization, Data curation, Funding acquisition, Investigation, Methodology, Project administration, Resources, Supervision, Validation, Writing - original draft, Writing - review & editing. **Farjad Shadmehri:** Supervision, Writing - review & editing. **Daniel Rosca:** Investigation, Methodology, Data curation, Writing - review & editing. **Ashraf Ahmed:** Investigation, Data curation, Writing - review & editing.

Declaration of Competing Interest

The authors declare that they have no known competing financial interests or personal relationships that could have appeared to influence the work reported in this paper.

Acknowledgement

Financial support from the Natural Sciences and Engineering Research Council of Canada and Bell Flight through the NSERC Industrial Chair on Automated Composites Manufacturing is appreciated.

Appendix A. Supplementary data

Supplementary data to this article can be found online at https://doi.org/10.1016/j.compstruct.2020.112097.

References

[1] Derisi B. Development of thermoplastic composite tubes for large deformation Ph.D thesis Concordia University; 2008.
[2] Derisi B, Suong H, Duosheng X, Hojjati M, Fews R. Composite Tube Exhibiting Large Deformation under Bending. J Compos Mater 2010;44:2005–20.
[3] Derisi B, Hoa S, Hojjati M. Similitude study on bending stiffness and behavior of composite tubes. J Compos Mater 2012;46:2695–710.

[4] Kollár L, Springer GS. Stress analysis of anisotropic laminated cylinders and cylindrical segments. Int J Solids Struct 1992;29:1499–517.
[5] Love AEH. A treatise on the mathematical theory of elasticity. Cambridge University Press; 2013.
[6] Tutuncu N, Winckler SJ. Stresses and deformations in thick-walled cylinders subjected to combined loading and a temperature gradient. J Reinf Plast Compos 1993;12:198–209.
[7] Hu G, Bai J, Demianouchko E, Bompard P. Mechanical behaviour of ± 55° filament-wound glass-fibre/epoxy-resin tubes—III. Macromechanical model of the macroscopic behaviour of tubular structures with damage and failure envelope prediction. Compos Sci Technol 1998;58:19–29.
[8] Bai J, Hu G, Bompard P. Mechanical behaviour of ± 55° filament-wound glass-fibre/epoxy-resin tubes: II. Micromechanical model of damage initiation and the competition between different mechanisms. Compos Sci Technol 1997;57:155–64.
[9] Lekhnitskii S, Fern P, Brandstatter JJ, Dill E. Theory of elasticity of an anisotropic elastic body. Phys Today 1964;17:84.
[10] Pagano NJ. The stress field in a cylindrically anisotropic body under two-dimensional surface tractions. Mechanics of composite materials. Springer; 1994. p. 151–6.
[11] Davies GC, Bruce DM. A stress analysis model for composite coaxial cylinders. J Mater Sci 1997;32:5425–37.
[12] Han H, Taheri F, Pegg N, Lu Y. A numerical study on the axial crushing response of hybrid pultruded and ± 45° braided tubes. Compos Struct 2007;80:253–64.
[13] Aksoy Ş, Kurşun A, Çetin E, Haboğlu MR. Stress analysis of laminated cylinders subject to the thermomechanical loads. World Acad Sci Eng Technol Int J Mech Aerospace Ind Mechatronic Manuf Eng 2014;8:244–9.
[14] Nowak T, Schmidt J. Theoretical, numerical and experimental analysis of thick walled fiber metal laminate tube under axisymmetric loads. Compos Struct 2015;131:637–44.
[15] Stockwell A, Cooper P. Collapse of composite tubes under end moments. 33rd Structures, Structural Dynamics and Materials. Conference 1992:2389.
[16] Chan WS, Demirhan KC. A simple closed-form solution of bending stiffness for laminated composite tubes. J Reinf Plast Compos 2000;19:278–91.
[17] Tarn J-Q, Wang Y-M. Laminated composite tubes under extension, torsion, bending, shearing and pressuring: a state space approach. Int J Solids Struct 2001;38:9053–75.
[18] Xia M, Takayanagi H, Kemmochi K. Bending behavior of filament-wound fiber-reinforced sandwich pipes. Compos Struct 2002;56:201–10.
[19] Arjomandi K, Taheri F. Bending capacity of sandwich pipes. Ocean Eng 2012;48:17–31.
[20] Menshykova M, Guz IA. Stress analysis of layered thick-walled composite pipes subjected to bending loading. Int J Mech Sci 2014;88:289–99.
[21] Sun X, Tan V, Chen Y, Tan L, Jaiman R, Tay T. Stress analysis of multi-layered hollow anisotropic composite cylindrical structures using the homogenization method. Acta Mech 2014;225:1649–72.
[22] Jonnalagadda A, Sawant A, Rohde S, Sankar B, Ifju P. An analytical model for composite tubes with bend–twist coupling. Compos Struct 2015;131:578–84.
[23] Ahmad MG, Hoa S. Flexural stiffness of thick walled composite tubes. Compos Struct 2016;149:125–33.
[24] Jolicoeur C, Cardou A. Analytical solution for bending of coaxial orthotropic cylinders. J Eng Mech 1994;120:2556–74.
[25] Akgun G, Algul I, Kurtaran H. Nonlinear Static analysis of laminated composite hollow beams with super-elliptic cross-sections. World Acad Sci Eng Technol Int J Mech Aerospace Ind Mech Manuf Eng 2017;11:1460–5.
[26] Yazdani Sarvestani H, Hojjati M. Effects of lay-up sequence in thick composite tubes for helicopter landing gears. Proc Inst Mech Eng Part G: J Aerosp Eng. 2017;231:2098–110.
[27] Zhang C, Hoa SV, Liu P. A method to analyze the pure bending of tubes of cylindrically anisotropic layers with arbitrary angles including 0 or 90. Compos Struct 2014;109:57–67.
[28] Hyer MW. Stress analysis of fiber-reinforced composite materials: DEStech. Publications Inc; 2009.
[29] Shadmehri F, Derisi B, Hoa S. On bending stiffness of composite tubes. Compos Struct 2011;93:2173–9.
[30] Librescu L, Song O. Behavior of thin-walled beams made of advanced composite materials and incorporating non-classical effects. Appl Mech Rev 1991;44:S174–80.
[31] Na S. Control of dynamic response of thin-walled composite beams using structural tailoring and piezoelectric actuation. Virginia Tech 1997.
[32] Reddy JN. Mechanics of laminated composite plates and shells: theory and analysis. CRC Press; 2004.
[33] Gay D, Hoa SV. Composite materials: design and applications. Second Edition CRC Press; 2007.
[34] Solvey Inc., www.solvey.com.